J. Fluid Mech. (1984), *vol.* 141, *pp.* 257–287
Printed in Great Britain

Two-phase displacement in Hele-Shaw cells: experiments on viscously driven instabilities

By C.-W. PARK, S. GORELL† AND G. M. HOMSY
Department of Chemical Engineering, Stanford University, Stanford, California 94305

(Received 21 June 1983 and in revised form 2 December 1983)

Corrigendum: Vol 144, 468–469

Experiments on the instability of the interface in two-phase displacements in Hele-Shaw cells were conducted using air and a viscous oil as the working fluids. The experiments had two objectives: (i) to provide quantitative measurements of the growth constants of the instability which occurs when a less-viscous fluid displaces a more-viscous one, and (ii) to compare the measured dispersion relations with the predictions of the recent theory of Park & Homsy (1984). The experiments were made by analysing the growth characteristics of between 10 and 20 Fourier modes describing the shape of the interface between displaced and displacing fluids, using still photography. For capillary numbers $Ca = \mu U/\gamma$ less than approximately 4×10^{-3} the agreement is only fair, owing to substantial edge effects produced by a nearly static contact line near the lateral boundaries of the cell. For $4 \times 10^{-3} < Ca < 1 \times 10^{-2}$ theory and experiment agree to within the accuracy of the measurements. Location and verification of the behaviour of modes near the predicted cut-off wavenumber give partial verification of the theory of Park & Homsy.

1. Introduction

The displacement of one fluid by another in a Hele-Shaw cell constitutes an important problem in fluid mechanics (Hele-Shaw 1898). Because of the well-known analogy between the depth-averaged velocity and pressure fields in a Hele-Shaw flow and two-dimensional flow in porous media (Stokes 1898; Lamb 1932), these experiments have been used to study and understand the stability of two-phase displacement processes in porous media. In addition to the mathematical analogy, the Hele-Shaw cell is a very simple, well-characterized system which, in contrast to a porous medium, provides good visibility of the flow motion. Thus many experiments have been performed in Hele-Shaw cells, with accompanying mathematical treatments (Saffman & Taylor 1958; Chouke, Van Meurs & Van der Poel 1959; White, Colombera & Philip 1976, 1977).

In an appendix to their paper, Saffman & Taylor showed that the analogy to porous-media flow applies even if a constant-thickness film of the displaced fluid is left behind the advancing meniscus between the fluids. At issue then are the jump or boundary conditions that hold at the interface.

Saffman & Taylor solved a two-dimensional potential problem to get the shape of the predominant single finger at steady state assuming continuity of pressure (minus the pressure jump across the meniscus) at the interface. There are an infinite number of solutions to this problem as posed. Selecting that solution corresponding to the observed ratio of finger to channel width yielded good agreement in the profile shape

† Present address: Shell Development Co., Houston, Texas.

when a modified capillary number is large. Considerable discrepancy occurs when the capillary number is small. In an attempt to remove the indeterminacy of the Saffman–Taylor solution, McLean & Saffman (1981) considered the effect of surface tension by adopting essentially the following *ad hoc* pressure-jump condition:

$$\Delta P = \gamma\left(\frac{1}{b}+\frac{1}{R}\right). \tag{1.1}$$

γ is the interfacial tension between the two fluids, b is the half-thickness of the Hele-Shaw cell and R is the radius of curvature of the projection of the tip of the advancing meniscus onto a horizontal plane. Pitts (1980) modified b with the thought that the transverse radius of curvature will be smaller than b because of the viscous traction. Even though his results match well with the experimental results, this was accomplished by introducing an adjustable parameter in an *ad hoc* fashion. McLean & Saffman (1981) also used a slight modification of (1.1) which takes into account the existence of a film of wetting fluid of constant thickness in the displaced region. Again the results predicting the finger width as a function of capillary number do not agree with experiment. They realized that these discrepancies may not be removed without solving the three-dimensional problem which will result in a correct pressure jump condition. Saffman (1982) discussed this pressure-jump condition from the point of view of dimensional analysis. Recently Park & Homsy (1984) solved a three-dimensional free-boundary problem in a Hele-Shaw cell by developing a double-expansion method in which the small parameters were the capillary number and the ratio of the two characteristic lengthscales: the transverse and lateral dimensions of the interface. An important assumption was that the wall of Hele-Shaw cells is completely wet by the displaced fluid. The result yields the pressure-jump condition across the interface, the *asymptotic* form of which is

$$\Delta P = \gamma\left(\frac{1}{b}+\frac{\pi}{4}\frac{1}{R}\right). \tag{1.2}$$

This result implies two important points. One is that, even though the flow is very slow and quasi-static, the *ad hoc* jump condition (1.1) is not applicable. The other is that (1.1) is a correct *form* for the pressure jump condition in Hele-Shaw cells when the relevant conditions of small capillary number, small lateral variation of the interface, and wetting of the displaced fluid, are satisfied. Even though (1.2) is not directly applicable to the Saffman–Taylor problem because it holds only when the lateral variation of the interface is small, its origin and derivation may shed some light on the intriguing fundamental discrepancy between theory and experiment as discussed by Saffman & Taylor (1958) and McLean & Saffman (1981).

The linear instability theory of one-dimensional displacement is well known (Chouke *et al.* 1959), and predicts the following dispersion relation:

$$\sigma(k)\left(\frac{\mu_1}{K_1}+\frac{\mu_2}{K_2}\right) = U\left(\frac{\mu_1}{K_1}-\frac{\mu_2}{K_2}\right)k-\gamma_e k^3. \tag{1.3}$$

Here μ is the viscosity, K represents the permeability and $\sigma(k)$ is the growth constant corresponding to a wavenumber k. In Hele-Shaw cells K_1 and K_2 become proportional to $\frac{1}{3}b^2$ as derived by Stokes (1898) and Saffman & Taylor (1958), and γ_e is $\frac{1}{4}\pi\gamma$ according to the recent work of Park & Homsy (1984). These results hold in the limit of zero capillary number.

Virtually all of the previous experiments on the viscous fingering instability in Hele-Shaw cells have been qualitative in nature. Most of these studies have compared

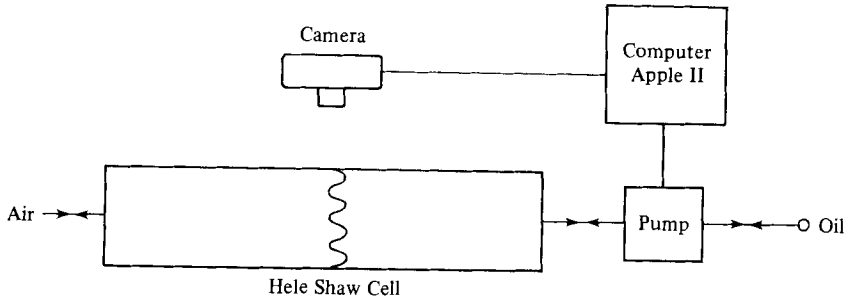

FIGURE 1. Schematic of the apparatus.

the observed nominal wavelength of the instability with the wavelength of the maximum growth rate given by a theory based on the *ad hoc* condition (1.1) (see e.g. Chouke *et al.* 1959; White *et al.* 1976, 1977; Gupta & Greenkorn 1974). When these comparisons are made, the agreement is fairly good. The reason for this can be seen by comparing the *ad hoc* condition (1.1) with the correct one (1.2). Since at low capillary numbers the two differ by only a factor of $\frac{1}{4}\pi$, the preferred wavenumber differs by a factor of $(\frac{1}{4}\pi)^{\frac{1}{2}}$. The experiments to date have not been sufficiently accurate to distinguish between the two results, but see the discussion of the data of White *et al.* (1976) in §4. To our knowledge, there have not been any attempts to measure the growth rates of the viscous instability.

Thus the objectives of our experiments were: (i) to measure growth rates and the dispersion relation over a range of capillary numbers, and (ii) to obtain, in so far as was possible, experimental corroboration of the correct boundary condition, (1.2).

2. Apparatus and procedure

Figure 1 represents a schematic of the apparatus, which has four main elements: the Hele Shaw cell, an oil pump, a microcomputer and a camera. The Hele Shaw cell consisted of two sheets of $\frac{1}{2}$ in. thick Pyrex plate glass separated by 2.5 cm wide flat rubber strips placed along the edges of the cell to serve as both a separator to maintain the gap thickness and a gasket to seal the edges. Two thicknesses of gaskets, approximately 0.06 and 0.08 cm, were used. The flow channel had nominal dimensions 120 cm in length and 20 cm in width. Individual bent aluminium strips were fabricated to act as clamps. These were glued every 11 cm along the sides of the top and bottom plates, and set so that holes for bolts on each matching top–bottom piece were aligned. Bolts were then placed in each clamp to keep the plates together with a uniform gap thickness. This arrangement allowed the cell to be dismantled for cleaning while maintaining an acceptable degree of reproducibility of experimental conditions. One end of the cell was open to the atmosphere while the other was fitted with a Plexiglas endpiece bolted to the glass and sealed with a silicone rubber gasket.

The pump was a Masterflex integral-drive variable-speed peristaltic pump (Cole–Parmer Model 7534-30), whose speed could be set manually or controlled by the microprocessor. Calibration of the pump for any of several removable pump heads resulted in a wide range of possible flow rates.

As noted, a microprocessor (Apple II-Plus) was available for control and subsequent data analysis. In addition, a real-time clock (Mountain Computer Co.) was available. A 35 mm SLR camera was mounted vertically above the Hele-Shaw cell and could be translated to a position directly above the interfacial position.

Run no.	h (cm)	U (cm/s)	μ (cP)	γ (dyn/cm)	$Ca = \mu U/\gamma$
1	0.08	0.060	77	30.7	1.5×10^{-3}
2	0.08	0.097	75.5	30.7	2.4×10^{-3}
3	0.056	0.052	230	31.3	3.8×10^{-3}
4	0.056	0.062	259	31.3	5.1×10^{-3}
5	0.08	0.090	222	31.3	6.4×10^{-3}
6	0.08	0.120	222	31.3	8.5×10^{-3}

TABLE 1

Air and oil were used as the two fluids, in order to assure that the displaced fluid wets the glass. Therefore the viscosity of the displacing fluid could be neglected.

Two different oils were used. One was Shell Carnea 100, which had a viscosity of 2.30 P and a surface tension of 31.3 dyn/cm at room temperature. The other was a blend of Shell Carnea 100 and Shell IVI 450, which had a viscosity of 0.75 P and a surface tension of 30.7 dyn/cm at room temperature. The viscosity and the surface tension were measured as functions of temperature using a Cannon–Fenske viscometer and a ring tensiometer respectively.

To measure the gap thickness, which is the most important dimension of the Hele-Shaw cell, we used an indirect method. The cell was tilted into a vertical position and filled with oil. The oil was then drained under gravity very slowly while the amount of oil collected over time and the corresponding locations of the air–oil interface were measured. A graph of the volume of the oil versus the location of the interface should be a straight line with the slope equal to the cross-sectional area. Since the width of the channel was 20 cm, the corresponding average gap thickness could be calculated through a linear-regression routine. The results gave 0.08 cm and 0.056 cm as the thicknesses of each rubber strip. The linear-regression coefficient of these data was 0.999, which is a measure of the uniformity of the gap thickness.

The experimental procedure was as follows. The cell, initially filled with oil, was tilted vertically so that gravity would help flatten the interface. It was then rotated slowly to a horizontal position while maintaining the flat interface. To produce the instability the oil was then pumped out at a steady rate through a Tygon tubing, which was connected to the Plexiglas endpiece. Still photographs were taken approximately every 10 s from the beginning of the displacement: only the initial stages of instability were studied here, in order to assure that the measurements were in the linear regime. The elapsed time associated with each picture was measured accurately using the clock of the Apple II computer, which was connected with the camera shutter switch by a simple electric circuit. Photographs were then enlarged to the size of approximately 20 cm × 25 cm to allow quantitative analysis of the growing instability.

Six experimental runs were made in which the oil viscosity, displacement velocity and gap thickness were all varied. The surface tension varied only slightly between the two oils, and cannot be considered as having been varied in this study. Table 1 gives the range of variables covered. As shown, the capillary number was varied from 1.5×10^{-3} to 8.5×10^{-3}.

3. Results and analysis

Two sets of experimental results appear in figure 2. Figure 2(*a*) shows the growth of the instability for $Ca = 1.5 \times 10^{-3}$ (run 1), and figure 2(*b*) shows that for $Ca = 8.5 \times 10^{-3}$ (run 6). We note from these photographs that the interface between air and oil was almost pinned at the two edges. This occurs because the rubber strips were readily wetted by the oil, and it undoubtedly leads to some error due to edge effects. Similar edge effects can be seen in the studies of White *et al.* (1976, 1977). In analysing the results we therefore eliminated at least 1.5 wavelengths at each edge from consideration and attempted to get as many fingers as possible, hopefully minimizing the edge effect. (We will refer to the nominal wavelength as W; see figure 3.) As we shall see this was not always successful, especially at low capillary number. The only way to get more fingers while keeping the capillary number small was to decrease the gap thickness, but this can only be done to a certain extent before gap non-uniformities would begin to significantly influence the results.

The photographs were analysed as follows. The picture corresponding to the initial interface was superposed on each photograph in a sequence. This resulted in a sequence of representations which showed the interface at both the initial and a later time. To minimize the edge effect, a portion of the picture near the edges was neglected and the remaining width D of the photograph, was discretized into N equally spaced points as shown schematically in figure 3. The distance between the initial and the displaced interface was then measured at each of the N points. These measured distances provided a record of the location of N material points and thus described the change in the shape of the interface as it was convected through the apparatus.

By applying a discrete Fourier transform (DFT) to this sequence of measured distances, the spectral components of the displaced interface were determined at each time. That is, the location of the interface at each time could be decomposed into the Fourier perturbation modes as follows:

$$f(t, z) = \sum_{m=0}^{\frac{1}{2}N} A_m(t) \exp\left\{i \frac{\pi m z}{D}\right\}, \tag{3.1}$$

where $f(t, z)$ represents the location of the interface as a function of time and position, and as noted D is the width over which the discretization was performed. Depending upon the importance of the edge effect, both D/L and W/L should be small. If the growth of disturbance is in the linear regime, $A_m(t)$ is given by

$$A_m(t) = a_m \exp\{\sigma_m t\}, \tag{3.2}$$

where a_m is a constant which is determined by the initial condition of the interface, and σ_m is the growth constant corresponding to the mode m. A semilogarithmic plot of $A_m(t)$ as a function of time should therefore yield a straight line, and the slope of it should be the growth constant σ_m. Figure 4 represents the semilog plot of $A_m(t)$ of the experimental result taken from run 4 for several wavenumbers. When this is done the lower modes may easily be identified as unstable. As can be seen from figure 4(*a*), the data points fit on straight lines, the linear regression coefficients of which were larger than 0.98, implying that the instability grows exponentially in time in accordance with the predictions of linear instability theory. Even though the three lines (1, 2, 3 of figure 4*a*) are almost straight with regression coefficients near unity, they seem to show a trend of becoming concave at later times which may represent the fact that they are becoming saturated, i.e. they are deviating from the linear regime. This phenomenon is more prominent for the faster-growing modes. For

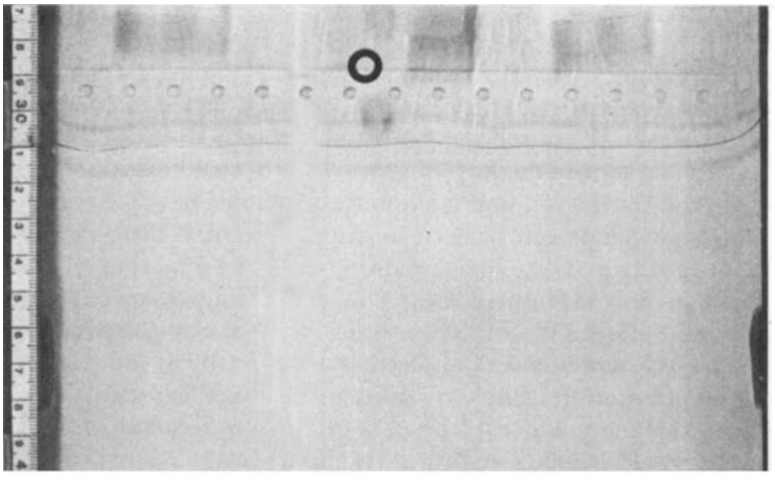

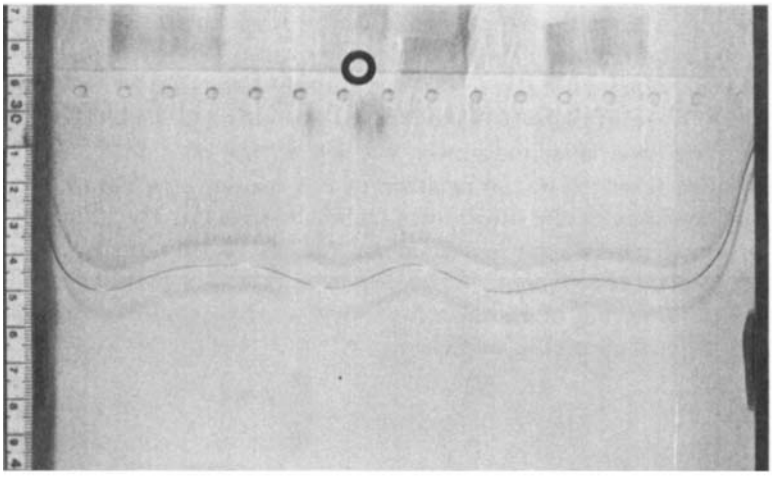

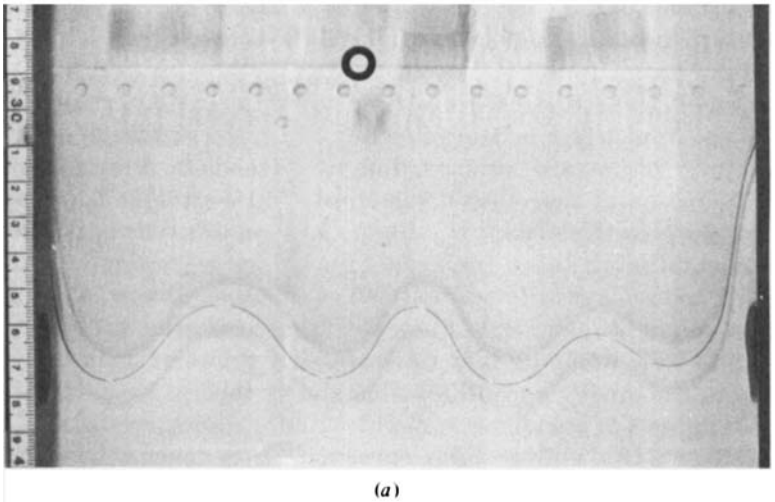

(*a*)

FIGURE 2(*a*). For caption see facing page.

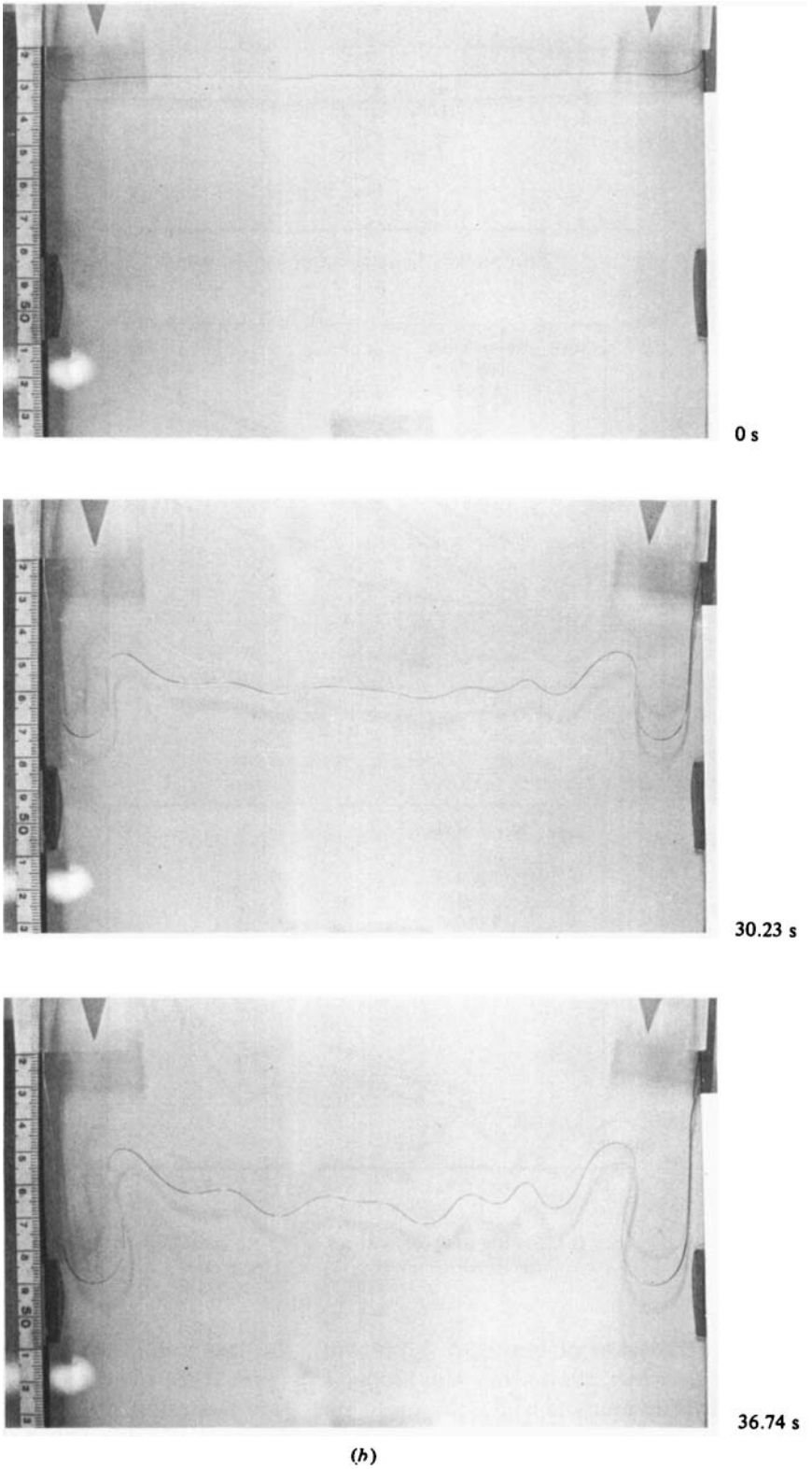

(*b*)

FIGURE 2. Instability of an air–oil interface; (*a*) run 1, $Ca = 1.5 \times 10^{-3}$; (*b*) run 6, $Ca = 8.5 \times 10^{-3}$; lower phase is oil.

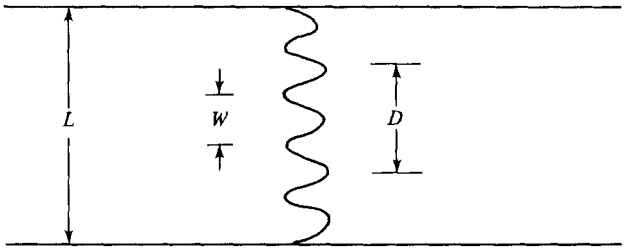

FIGURE 3. Schematic of a displacement.

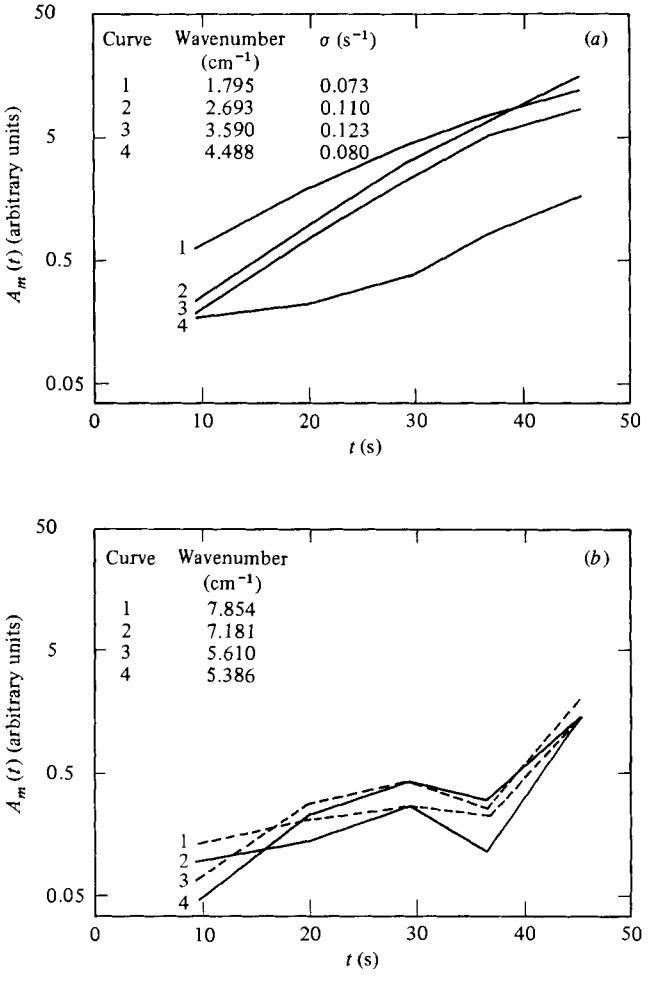

FIGURE 4. Growing and neutral modes of an instability (run 4): (*a*) growing modes; (*b*) neutral modes.

example, in the case of line 3 of figure 4(*a*), the last point was eliminated from consideration when computing the slope. In figure 4(*b*), even though the mode amplitudes, the values of which are quite small, are less reliable, it can be said that each mode does not exhibit sustained exponential growth, implying that these modes are neutrally stable. In this point of view, mode 4 (4 of figure 4(*a*)), which starts to

deviate from exponential growth, may be near the cutoff wavenumber. Thus such semilogarithmic plots can be used to discriminate easily between unstable and stable modes. The stable modes appear nearly neutral and not damped owing to the constant occurrence of noise and small perturbations in the system.

The average velocity U of the interface was calculated from the data of $A_0(t)$ versus time. Because $A_0(t)$ represents the averaged location of the interface as a function of time, a plot of $A_0(t)$ versus t yields a straight line, the slope of which is the average velocity of the interface. Thus U was calculated by a linear-regression routine, and the linear-regression coefficient was always larger than 0.99 for every run. The total amount of oil pumped out during the experiment was measured to calculate the flow rate, which gives the average velocity when divided by the cross-sectional area. Therefore the average velocity calculated from the zero harmonic could be checked by comparing it with that calculated from the amount of oil collected. The difference between them was less than 5% in all cases.

The linear dispersion relation is, from (1.3),

$$\frac{12}{d^2}\sigma_k(\mu_1+\mu_2) = \frac{12U}{d^2}(\mu_1-\mu_2)\,k-\frac{\pi}{4}\gamma k^3, \tag{3.3}$$

where d is the gap thickness of the Hele-Shaw cell and σ_k is the growth constant corresponding to the wavenumber k. As explained above, (3.3) holds only in the limit of small capillary number. Because the displacing fluid was air, μ_2 is negligible compared with μ_1, the viscosity of the oil. Thus $\mu_2 \approx 0$, and we set $\mu_1 = \mu$. The relation between the harmonic number m and the wavenumber k is given by

$$k = \frac{2\pi m}{D}. \tag{3.4}$$

Therefore the dispersion relation (3.3) becomes

$$\sigma_{\mathrm{m}} = \frac{2\pi U}{D}m-\frac{\pi^4 d^2\gamma}{6\mu D^3}m^3. \tag{3.5a}$$

Because each quantity in (3.5a) is known, the experimental results for σ_m can be compared with the theory. Since (3.5a) can be rewritten as

$$\frac{d}{U}\left(\frac{\gamma}{\mu U}\right)^{\frac{1}{2}}\sigma_m = 2\pi\frac{d}{D}\left(\frac{\gamma}{\mu U}\right)^{\frac{1}{2}}m\left\{1-\frac{\pi}{48}\left(2\pi\frac{d}{D}\left(\frac{\gamma}{\mu U}\right)^{\frac{1}{2}}m\right)^2\right\}, \tag{3.5b}$$

it is possible to represent the results in normalized form, in which σ and m are scaled as follows:

$$\sigma = \frac{d}{U}\left(\frac{\gamma}{\mu U}\right)^{\frac{1}{2}}\sigma_m \tag{3.5c}$$

$$\alpha = 2\pi\frac{d}{D}\left(\frac{\gamma}{\mu U}\right)^{\frac{1}{2}}m. \tag{3.5d}$$

Therefore the normalized dispersion relation becomes

$$\sigma = \alpha\left(1-\frac{\pi}{48}\alpha^2\right). \tag{3.5e}$$

Figure 5 shows the normalized dispersion relations shown as a solid curve, together with the experimental results. Also shown in the figure is an arrow on the abscissa, giving the normalized cut-off wavenumber given by the *ad hoc* expression (1.1). For

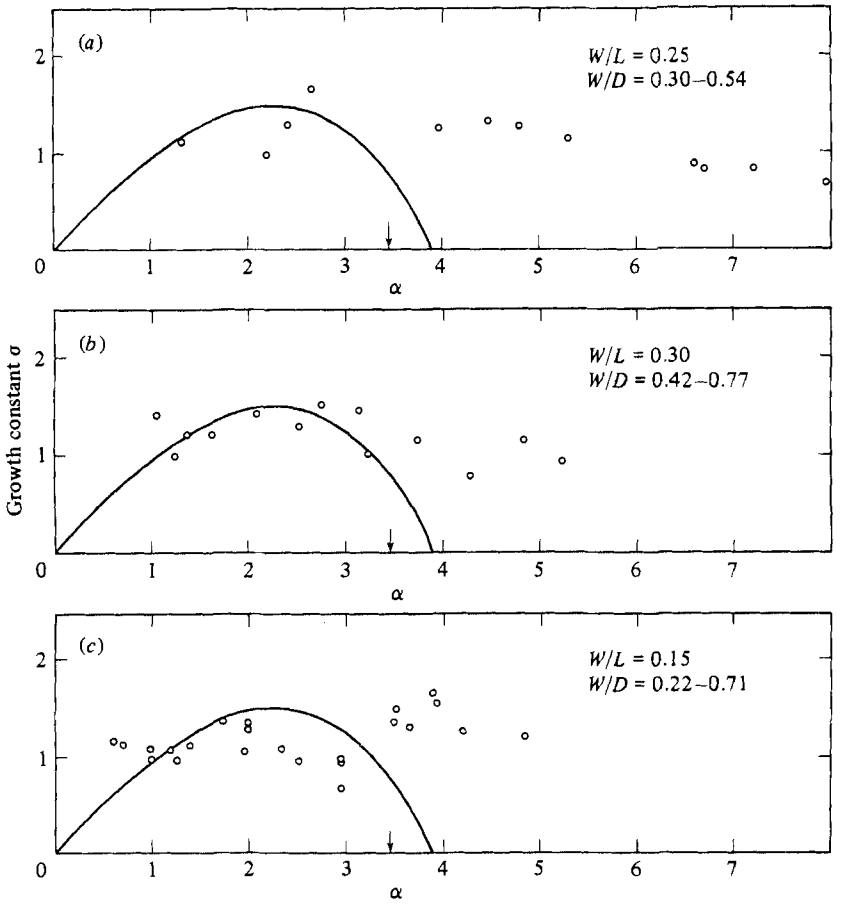

FIGURE 5(a–c). For caption see facing page.

each run, W/L and W/D are specified in the figures. Implications of figure 5 are discussed in §4. Table 2 shows the information taken from the replicate analyses of run 3 by slightly shifting the analysis region D in order to make approximate estimates of probable errors in α and σ. In (3.5*c*, *d*) d, γ, μ and D are fixed. Therefore table 2 gives the approximate error due to the measurements of the displacement of the interface. Since the difference in α comes from the difference in U, the average velocity of the interface, which was calculated from zero harmonic as explained, only one datum is actually given in table 2, even though four data are listed. The average velocities for each analysis were 0.052 cm/s and 0.053 cm/s, and they made a 1.3 % relative error in α.

In case of $|\Delta\sigma|$, since the two sets of analyses were performed for four modes, four data are available as listed in table 2. They indicate a probable error of approximately 10 % in the measurement of growth constants.

4. Discussion and conclusion

Figure 5 shows that at capillary numbers that are larger than about 5×10^{-3} (figures 5*d–f*) the experimental results agree well with theory but at the smaller capillary numbers (figures 5*a–c*) they show discrepancies, i.e. the modes of high wavenumbers,

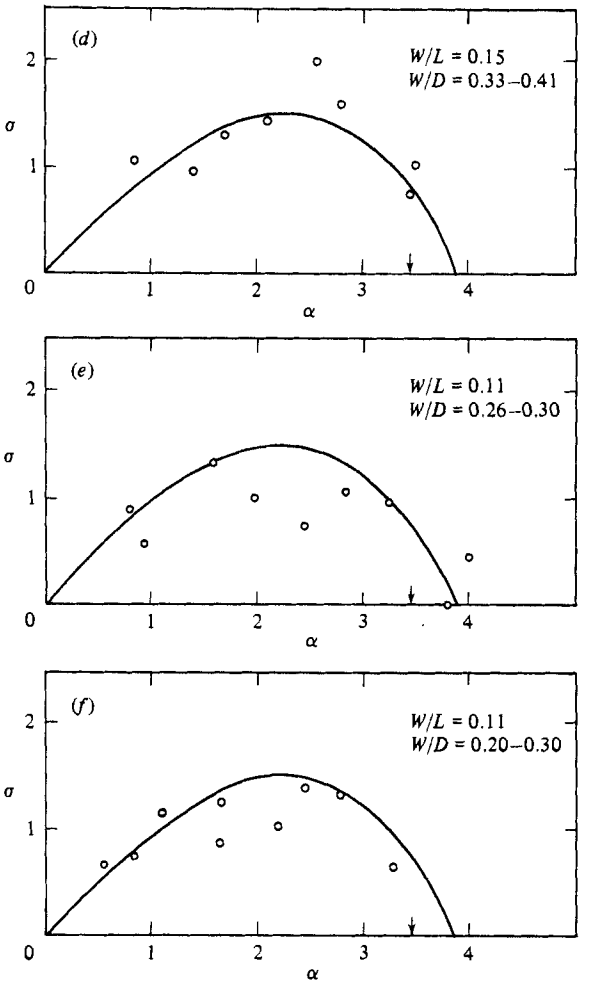

FIGURE 5. Normalized dispersion relations.

m	α_1	α_2	$\Delta\alpha$	σ_1	σ_2	$\lvert\Delta\sigma\rvert$
1	0.981	0.968	0.013	1.066	0.947	0.119
2	1.961	1.936	0.025	1.275	1.032	0.243
3	2.942	2.904	0.038	0.943	0.677	0.266
4	3.923	3.872	0.051	1.520	1.658	0.138

TABLE 2

which are larger than the theoretical cut-off wavenumber, are also growing, even though the order of magnitude of the growth constants agrees with theory. These discrepancies are more prominent as the capillary number decreases or as the value of W/L increases. This was puzzling to us at first, since the theory is asymptotically correct as $Ca \to 0$. A possible explanation for these discrepancies is as follows. At low capillary numbers, two effects need to be considered which would be absent in an apparatus of very large horizontal extent. First, the number of fingers is small, and, secondly, the growth constant is lower the smaller the capillary number. These effects

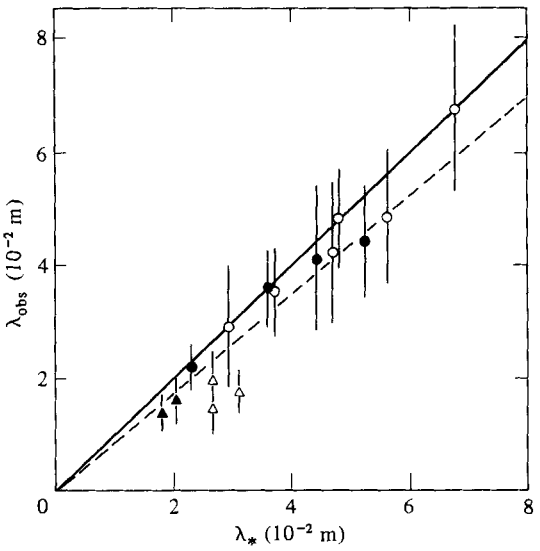

FIGURE 6. Comparison of the observed wavelengths with theoretical ones ($Ca = 10^{-3}$–10^{-2}) (taken from White *et al.* 1976).

make themselves felt as follows. As mentioned above, the interface stayed nearly fixed at the edges of the cell, leading to an edge effect which may be minimized but never completely eliminated. Obviously, the number of fingers must be fairly large for the experiment to be a good approximation to being infinite in lateral extent, i.e. W/L must be small. The other way in which the edge effect enters is more subtle. Since the dimensional growth constant becomes small at small Ca, a long period of time must pass in order to obtain measurable growth of disturbances relative to the uniform displacement of the interface. But, since the edge of the interface is nearly pinned, the displacement is not laterally uniform, which obviously influences the events toward the centre of the domain. Conversely, both the value of W/L and the time over which measurable growth occurs decrease with increasing capillary number, leading to a minimization of the edge effect.

Both these factors are clearly shown in figure 2, where at the smallest value of Ca there are only three wavelengths and substantial growth occurs over $\sim$ 110 s, while at the largest value of Ca roughly 6–11 wavelengths exist and the growth occurs over $\sim$ 40 s. Thus we consider the very-low-Ca data to be inaccurate for these two reasons, and good experimental accuracy is a compromise between the need to operate at low Ca where the theory applies and higher Ca where the edge effects may be minimized. The data shown in figure 5 together with the visualizations tend to corroborate this explanation, as the trends are consistent with it.

Considering the data in figures 5(*d–f*), we note that although the accuracy in σ is low the general trend of the data is correct. Furthermore, recalling that the semilogarithmic plots can readily distinguish unstable from stable modes, we have at least five instances of observing unstable modes which would be damped according to the *ad hoc* boundary condition. We consider this to be evidence for the correctness of (1.2), but the data are not accurate enough to distinguish unequivocally between the two predictions.

Therefore we can conclude that for the intermediate capillary numbers ($Ca > 5.1 \times 10^{-3}$) at which we could minimize the edge effect

(i) σ is in reasonable agreement with theory,

(ii) positive σ near the cut-off corroborates the theory of Park & Homsy,

(iii) no modes grow above the cut-off wavenumber.

A survey of experiments performed by previous investigators in Hele-Shaw cells yields evidence which is relevant to our recent work. Chouke *et al.* (1959) did some experiments to verify their theory. White *et al.* (1976, 1977) also performed many Hele-Shaw experiments to study the stability problem in a porous medium. In comparing results with theory, both assumed the *ad hoc* boundary condition (1.1). They measured the average finger spacing, which they assumed to correspond to the wavelength of the maximum growth rate, and compared it with their theoretical calculations. Although there is nominally good agreement between their theories and experiments, careful investigation of their experimental results indicates that their theories always overestimated the wavelength of the maximum growth rate. According to our recent work, the wavelength of maximum growth rate is $(\frac{1}{4}\pi)^{\frac{1}{2}}$ times that of their theories, implying that the correct wavelength is 11 % smaller than calculated. Figure 6, taken from the experiments of White *et al.* (1976), the capillary numbers of which were between 10^{-3} and 10^{-2}, shows that, although the errors in this kind of measurement are large, the observed wavelength is consistently below that given by the *ad hoc* theory. The correct theory is shown as the dashed line $\lambda_{\text{obs}} \approx 0.89\lambda_*$, and the data would appear to support our theory.

This work was supported by the U.S. Department of Energy, Office of Basic Energy Sciences.

REFERENCES

CHOUKE, R. L., VAN MEURS, P. & VAN DER POEL, C. 1959 The instability of slow, immiscible, viscous liquid–liquid displacements in permeable media. *Trans. AIME* **216**, 188.

GUPTA, S. P., VARNON, J. E. & GREENKORN, R. A. 1974 Viscous finger wavelength degeneration in Hele-Shaw models. *Water Resources. Res.* **9**, 1039.

HELE-SHAW, H. S. 1898 Stream-line motion of a viscous film. *Rep 68th Meeting Brit. Assoc.* p. 136.

LAMB, H. 1932 *Hydrodynamics*, 6th edn. Cambridge University Press.

MCLEAN, J. W. & SAFFMAN, P. G. 1981 The effect of surface tension on the shape of fingers in a Hele Shaw cell. *J. Fluid Mech.* **102**, 455.

PARK, C.-W. & HOMSY, G. M. 1984 Two-phase displacement in Hele Shaw cells: theory. *J. Fluid Mech.* **139**, 291.

PITTS, E. 1980 Penetration of fluid into a Hele Shaw cell: the Saffman–Taylor experiment. *J. Fluid Mech.* **97**, 53.

SAFFMAN, P. G. 1982 Fingering in porous media. In *Macroscopic Properties of Disordered Media* (ed. R. Burridge, S. Childress & G. Papanicolaou). Lecture notes in Physics, vol. 154, p. 208. Springer.

SAFFMAN, P. G. & TAYLOR, G. I. 1958 The penetration of a fluid into a porous medium or Hele-Shaw cell containing a more viscous liquid. *Proc. R. Soc. Lond.* **A245**, 312.

STOKES, G. G. 1898 Appendix to Hele-Shaw (1898).

WHITE, I., COLOMBERA, P. M. & PHILIP, J. R. 1976 Experimental study of wetting front instability induced by sudden change of pressure gradient. *Soil Sci. Soc. Am. J.* **40**, 824.

WHITE, I., COLOMBERA, P. M. & PHILIP, J. R. 1977 Experimental studies of wetting front instability induced by gradual changes of pressure gradient and by heterogeneous porous media. *Soil Sci. Soc. Am. J.* **41**, 483.